Preparation of the Spin-Mott State: A Spinful Mott Insulator of Repulsively Bound Pairs

Julius de Hond, Jinggang Xiang (□□□), Woo Chang Chung, Enid Cruz-Colón, Wenlan Chen, William Cody Burton, Colin J. Kennedy, and Wolfgang Ketterle

Phys. Rev. Lett. **128**, 093401 — Published 28 February 2022

DOI: 10.1103/PhysRevLett.128.093401

Preparation of the spin-Mott state: a spinful Mott insulator of repulsively bound pairs

Julius de Hond, Jinggang Xiang (项晶罡), Woo Chang Chung,* Enid Cruz-Colón,
Wenlan Chen,† William Cody Burton,‡ Colin J. Kennedy,‡ and Wolfgang Ketterle
Research Laboratory of Electronics, MIT-Harvard Center for Ultracold Atoms, Department of Physics, Massachusetts Institute of Technology, Cambridge, Massachusetts 02139, USA

We observe and study a special ground state of bosons with two spin states in an optical lattice: the spin-Mott insulator, a state that consists of repulsively bound pairs which is insulating for both spin and charge transport. Because of the pairing gap created by the interaction anisotropy, it can be prepared with low entropy and can serve as a starting point for adiabatic state preparation. We find that the stability of the spin-Mott state depends on the pairing energy, and observe two qualitatively different decay regimes, one of which exhibits protection by the gap.

Mott insulator states of ultracold atoms in optical lattices have played a central role in ultracold atoms research [1, 2]. Because they are a well-isolated low-entropy state protected by an energy gap, such states have been considered as qubits [3], as a starting point for adiabatic state preparation [4, 5], and for studies of many-body physics [6], in particular quantum magnetism [7]. They were used in seminal work on Heisenberg spin Hamiltonians [8–10] and as a platform to study Rydberg crystals [11] and magnetic polarons [12].

When the spin degree of freedom is added to a Mott insulator, it opens up low-lying excitations, and much lower temperatures are needed to reach the ground state. For occupations of $N = 1$, the energy scale is set by superexchange, the process by which two spins can be swapped via a virtual intermediate state. This energy scale is often smaller than 1 nK (e.g. for rubidium). As a result, magnetically ordered ground states were only observed using fermionic lithium (which due to its low mass has comparatively large tunneling and exchange energies) [13] or using special ramping schemes [14, 15].

Because preparing spinful ground states is challenging, many experiments probed spin dynamics through quenches, where an initial spin-polarized state is suddenly rotated into a spin superposition. This has enabled study of transport of bound states [17] and spin waves in isotropic [18] and anisotropic [19, 20] $S = 1/2$ Heisenberg models. Recently, we have also studied the relaxation of rotated spin states in $S = 1$ Heisenberg models [21]. Parallel efforts have succeeded in preparing bipartite product states through carefully shaped ramps [22, 23].

Here we show that the situation is drastically different for a spinful Mott insulator with two particles per site. If the on-site interaction energy U_{AB} between opposite spins is considerably lower than that between identical spins (U), there is an effective pairing energy $D = U - U_{AB}$ favoring the formation of repulsively bound pairs of opposing spins. The ground state of the $N = 2$ Mott insulator, then, is a Mott insulator of spin-paired doublons with an excitation gap D. This implies that a spinful $N = 2$ Mott insulator has a region in its phase diagram where the excitation gap is of scale D or U, which typically corresponds to 50 nK for rubidium, and is thus much larger than the superexchange scale (see Fig. 1). As a function of D, there is a phase transition in the spin domain between a spin superfluid (also known as a counterflow superfluid) and a spin insulator. This is in full analogy with the superfluid-to-Mott insulator transition in the charge domain [16]. The spin-Mott state can serve as an ideal starting point for adiabatic preparation of states with different spin ordering [4]. It is also analogous to the band insulator of fermions for $N = 2$ occupation [5], since this state is (in the limit of large pairing energy) a product state of spin-paired doublons on each site.

In this Letter, we demonstrate techniques to prepare and probe the spin-Mott state and study its stability. Our system comprises two different hyperfine states of ^{87}Rb in a (spin-dependent) optical lattice, which are described by the two-component Bose–Hubbard Hamiltonian [24]. In one dimension, and assuming equal tunneling for both components, this is given by:

$$H = -t \sum_i \left(a_i^\dagger a_{i+1} + b_i^\dagger b_{i+1} + \text{H.c.} \right) + \frac{U}{2} \sum_i \sum_{k \in \{a,b\}} n_i^k \left(n_i^k - 1 \right) + U_{AB} \sum_i n_i^a n_i^b. \quad (1)$$

Here n_i^k is the number operator acting on component k on site i, t is the nearest-neighbor tunneling parameter; U and U_{AB} are the intra- and interspecies on-site interactions, respectively, where we have assumed $U = U_{AA,BB}$.

Restricting ourselves to a deep lattice with two particles per site, this model maps onto an $S = 1$ Hamiltonian [4, 24], with the spin-Mott insulator as the ground state for $U_{AB} \ll U$. This is a product state with a single A and B atom per site, which in the spin mapping corresponds to $|S_z = 0\rangle$.

Correlations become important when the pairing and superexchange energy become comparable: $D \approx J \equiv -4t^2/U_{AB}$ [21, 25, 26]; in this regime second-order tunneling induces quantum fluctuations of the spin around the spin-Mott insulator. Here the ground state is an xy ferromagnet that contains correlations between sites

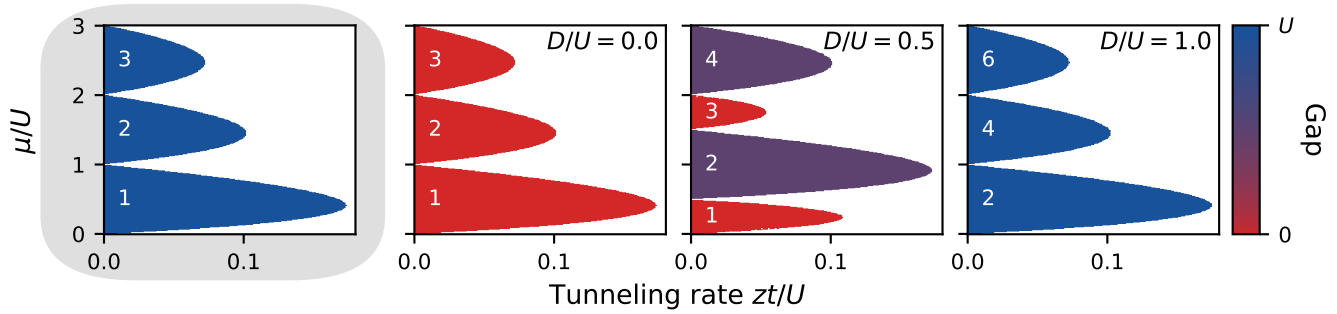

FIG. 1. Mean-field phase diagram of the (two-component) Mott insulator showing the number of atoms per site for a chemical potential μ and tunneling rate t (which, in the mean-field model, is enhanced by the coordination number z). The leftmost panel contains the phase diagram of the single-component system [16]. The other panels, from left to right, show the two-component phase diagram for $D/U = 0$, 0.5, and 1.0. As D increases, the lobes with an uneven number of particles shrink, until they vanish because the absence of interactions leads to the formation of two independent Mott insulators. The lobe color indicates the excitation gap. In the single-component system the first-excited state is a particle-hole pair, which costs an energy U to create. In the two-component system it is a spin excitation with an energy on the order of D. The numbers in the lobes indicate $\langle n \rangle = \langle n^a \rangle + \langle n^b \rangle$.

[4]; this bears resemblance to the superfluid phase of the single-component system, where the excitation gap vanishes, and where number fluctuations drive correlations between sites [16].

Experimental setup Our experiment starts with a Bose–Einstein condensate (BEC) of approximately 10^4 atoms. A mixture of the hyperfine states $A = |F = 1, m_F = -1\rangle$ and $B = |F = 1, m_F = 1\rangle$ is created using microwave sweeps, after which the cloud is loaded into a three-dimensional lattice with depths of at least $25E_R$ to be deep in the Mott-insulating regime. Here $E_R = h^2/2m\lambda^2$ is the recoil energy of a lattice photon with wavelength λ for an atom of mass m. The interaction between different hyperfine states of rubidium is nearly isotropic [27, 28], and hence for any pair $D \approx 0$. The interaction scale U_{AB} can be adjusted, however, by separating the Wannier functions of A and B atoms in the lattice. This can be done using spin-dependent potentials based on the vector AC Stark shift, which separates spin states with different magnetic moments. We create such a lattice using a 810-nm wavelength laser and a tunable polarization gradient [29]. The two transverse lattices are created using 1064-nm light.

Preparing the spin-Mott insulator For $D \approx U$, the absence of interspecies interactions leads to the formation of two independent Mott insulators (see Fig. 1). Here the system exhibits a large excitation gap which we have measured through lattice modulation [29]. This is similar to the single-component case which has a gap of U; hence it is straightforward to prepare the ground state of the Hamiltonian (1). We do so by creating an equal mixture of the two components, followed by a ramp of the lattice while maintaining $D \approx U$. If the atom number is adjusted to fall within the $N = 2$ Mott insulator plateau (but such that it avoids the $N = 3$ sector), we prepare a highly ordered spin state with the same wave function

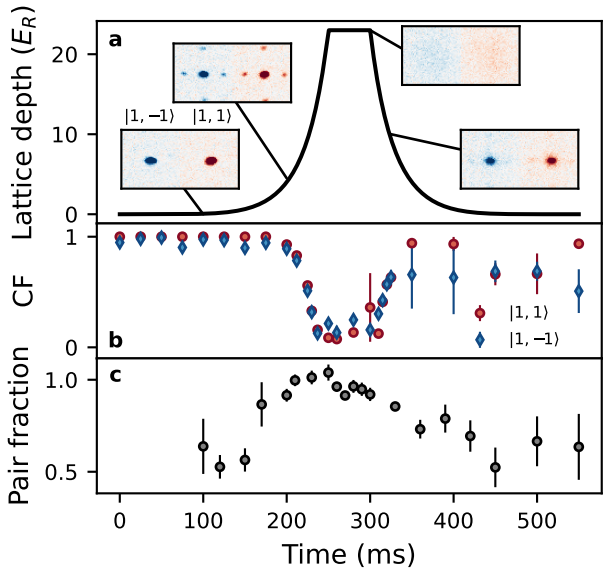

FIG. 2. The superfluid-to-Mott insulator phase transition for a system with two spin states. Starting with a spinor BEC in an equal superposition state of $|1, -1\rangle$ and $|1, 1\rangle$, we ramp up the lattice into the Mott-insulating regime while $D = U$ (**a**). In the Mott plateau we observe a dip in condensate fraction (CF, **b**), while the pairing fraction (**c**) approaches unity.

on every site.

The pairing fraction is measured using the detection protocol as described in Ref. [21]; in short, we quench to $D = 0$ (see insets in Fig. 3), and take three measurements using absorption imaging: one of the total atom number, one of the atom number after removing all pairs using a Feshbach resonance, and one after selectively removing just the AB pairs using a Feshbach resonance [30]. The removal procedure has been measured to saturate the losses over the time during which it is applied, from

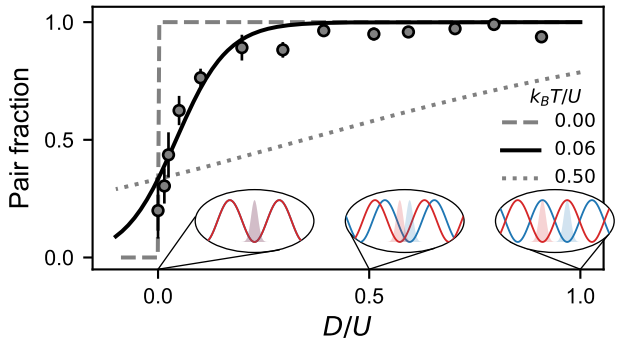

FIG. 3. Preparation of the spin-Mott state for various pairing energies D. The decrease of the spin pairing fraction for small D is explained by a finite temperature. Lines are based on the model of Eq. (2) at various temperatures. Insets: lattice configuration at various values of D/U.

which we conclude it to be efficient. The pairing fraction is given by the ratio of differences of these measurements, which makes it susceptible to shot-to-shot number fluctuations. To mitigate this, all data presented throughout is obtained as the average of three measurements in each of the three channels, with the error bar reflecting the standard error of the mean. Our measurement protocol directly determines the spin temperature of the system. It is not affected by holes and singly-occupied sites (it is affected by triplons, which we minimize by our state preparation protocol).

To highlight the correspondence between the spin-Mott insulator and its single-component cousin, we have measured the characteristic superfluid-to-Mott insulator phase transition [31]. Both components were imaged individually using Stern–Gerlach separation during time of flight, see Fig. 2. From these images, we can determine the condensate fractions in each state. Using our pair measurement protocol, we verify that the spin-Mott insulator (realized for deep lattices) has a pairing fraction close to unity.

The gap of the spin-Mott state shrinks as D is decreased. We have explored how small D can become before we observe a degradation of the spin-Mott state due to finite temperature or non-adiabatic loading. Figure 3 shows the initial pairing fraction as a function of D, after ramping into a deep lattice (23 E_R). We find that it is possible to attain high pairing fractions of over 0.9 for a wide range of initial values of D.

According to matrix-product-state calculations, the spin-Mott state is the ground state for $D > 0.05U$ at a lattice depth of 8 E_R [4]. The imperfect pairing fraction observed for $D < 0.2U$ in a 23 E_R lattice can be explained by finite spin temperature. We can deduce the temperature from a model where tunneling is assumed to be negligible, and hence the Hamiltonian is diagonal on each site in the basis $\{|AA\rangle, |AB\rangle, |BB\rangle\}$. Generalizing the treatment of a single-component Mott insulator [32], we obtain the pairing fraction (i.e. the population in $|AB\rangle$), for a thermal state $|\psi_T\rangle$ at temperature T as

$$|\langle AB|\psi_T\rangle|^2 = \left[1 + 2\exp\left(-D/k_BT\right)\right]^{-1}. \qquad (2)$$

Fitting this expression to our data, we obtain $k_BT/U \approx 0.06 \pm 0.01$, which corresponds to 4 ± 1 nK for $U/2\pi \approx 1300$ Hz. This is comparable to temperatures reported for single-component Mott insulators [33, 34]. We expect that the charge temperature (set by defects) and the spin temperature are in equilibrium during the lattice ramp while tunneling is fast. After loading, the charge temperature increases by diffusion of defects from outer parts of the cloud, while the spin temperature is protected as long as $D \gg t$ (see Fig. 4). The latter is lower than the temperature of the initial BEC due to adiabatic cooling during the lattice ramp [4]. Figures 2 and 3 represent the main result of this paper: the successful preparation of the ground state of a spinful $N = 2$ bosonic Mott insulator which has not been accomplished before.

Relaxation behavior The decay of the spin-Mott state determines how it can be used as a low-entropy starting point for further experiments. To investigate this, we measure the lifetime as a function of lattice parameters. After the preparation, we ramp D during 100 ms while staying in a deep (25 E_R) lattice – this can be considered a quench since the tunneling rate is on the order of 1 Hz. We then lower the lattice to 16 E_R and measure how the pairing fraction decays.

We can distinguish two qualitatively different relaxation regimes as a function of D, see the top panel in Fig. 4. When quenching D close to 0, the system quickly approaches the thermal state: an incoherent equal mixture of $|AA\rangle$, $|AB\rangle$, and $|BB\rangle$ on every lattice site, which leads to a pairing fraction of 1/3. For larger values of D the behavior is qualitatively different: not only does the relaxation take longer, the pairing fraction also does not decay to 1/3 over experimentally accessible timescales, rather it goes to $\sim 1/2$. This is what one would expect if thermalization were constrained to the symmetric subspace; i.e. the states $|AB\rangle$ and $(|AA\rangle + |BB\rangle)/\sqrt{2}$ with each receiving half the population. If all couplings preserve the initial symmetry, the system is constrained to this subspace.

The two different regimes also show up in the relaxation behavior as a function of lattice depth. In the bottom panels of Fig. 4 we compare the system when held in the spin-Mott phase and after quenching to $D = 0$. For small values of D, the decay rate scales linearly with the tunneling rate, while in the spin-Mott state the decay rate is lattice-depth independent.

This behavior is captured by modelling the total decay rate as the sum of a background contribution and a term that depends linearly on tunneling but which is suppressed by D:

$$\Gamma(t, D) = \Gamma_0 + (t/2\pi) / \left[1 + c_1 \exp\left(D/c_2\right)\right]. \qquad (3)$$

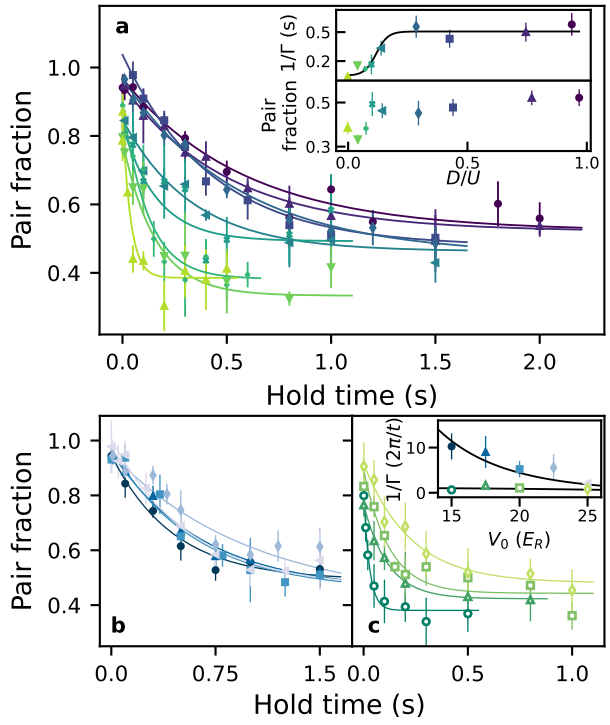

FIG. 4. Lifetime of the spin-Mott insulator. (**a**) The relaxation shows qualitatively different behavior as a function of D: The pair fraction either approaches the infinite temperature limit (1/3, if D is small) or not (1/2, if D is large). Different colors represent different values of D/U. Inset: fitted lifetimes $1/\Gamma$ and the equilibrium values of the pair fraction. (**b**, **c**) Lifetime at various lattice depths, represented by different colors, where D is fixed to be either within the spin-Mott insulator ($D = 0.3U$, **b**) or at the isotropic point where $D = 0$ (**c**). Inset: fitted lifetime for both data sets scaled by the tunneling time $2\pi/t$. For $D = 0$ we observe that the decay scales with tunneling, whereas for $D = 0.3U$ it is independent of t. A single fit of all the lifetimes was done using Eq. (3), which is shown by the black lines.

Here c_1 and c_2 are fit parameters, and the form is such that $\Gamma(t, D) \to \Gamma_0$ if D is large, as it is in the spin-Mott insulator. This expression gives us a quantitative description of the lifetimes measured in Fig. 4 (see Ref. [29]).

We conjecture that a combination of factors causes this. For $D \approx 0$ we enter the regime where the temperature of the $N = 2$ plateau is sufficiently large to drive deviations from perfect pairing already observed during loading (see Fig. 3). First-order tunneling with imperfections in the Mott insulator will allow entropy transport from the outer regions of the system inwards, which will rapidly increase the spin temperature. This is a plausible explanation for the scaling with tunneling rate.

At higher values of D the excitation gap protects against relaxation. It is seen through longer lifetimes that are lattice-depth independent. This makes it unlikely that the decay is caused solely by either tunneling or light scattering-related mechanisms. This is confirmed by a measurement of a spin-polarized Mott insulator which *does* show a scaling of lifetime with lattice intensity. Nevertheless, the interplay between different effects in our experiment is complicated; increasing the lattice depth increases both light scattering and confinement. With our current setup it is hard to disentangle such mechanisms. The cause of the slow spin relaxation could be mobile atoms in excited bands created by technical noise of the lattice beams, or grazing collisions with background gas atoms.

Discussion & conclusions While the spin-Mott insulator is a product state, it can be used as a starting point for adiabatically preparing correlated spin states such as the xy ferromagnet [4, 24]. Similar schemes have been proposed for fermions, where the (gapped) band insulator can be used to adiabatically prepare an antiferromagnet [5]. In that case the initial product state is stabilized by the bandgap, whereas in our case it is stabilized by the pairing energy D. This difference in energy scales also makes our system suitable for studying spin-charge separation [35].

Adiabatic state preparation requires that the gaps between many-body states are traversed sufficiently slowly; in a Landau–Zener model of avoided crossings, the maximum rate is set by the coupling between states [36–38]. In a deep lattice this scales with second-order tunneling as $\propto 4t^2/U$ [4, 21, 25]. Furthermore, coupling between different many-body states scales inversely with the number of sites in a chain. For our present system the superexchange scale is maximally 10 Hz at a longitudinal lattice depth of $12E_R$. This is comparable to some of the decay rates reported in Fig. 4. Therefore, attempts to adiabatically sweep the spin-Mott state into correlated spin states were not successful.

Other atomic species are favorable; cesium, e.g., has a larger fine-structure splitting which makes it possible to create a spin dependent potential at larger detunings with less light scattering. The lanthanides are also attractive because they feature spin-orbit coupling in the ground state, and hence have a vector AC Stark shift for any lattice detuning.

The future addition of a quantum-gas microscope to our setup [39] will mitigate some of these issues. With single-site resolution, experiments can be performed on short chains with definite length which are fully decoupled from surrounding thermal reservoirs.

In conclusion, we have prepared and characterized the spin-Mott state which is the ground state of the two-component Bose–Hubbard model in deep lattices, which can be mapped onto an $S = 1$ Heisenberg Hamiltonian. This state features a large pairing gap, and is a promising platform for adiabatic preparation of magnetic phases and the study of other many-body phenomena. Additionally, since the spin-Mott state is a product state of repulsively bound pairs it offers a way to study pair superfluidity [40, 41] and quantum droplets [42]. Analogous

to Ref. [43], one could do this by creating a dilute gas of repulsively bound dimers after reducing the harmonic confinement and emptying out the singly-occupied sites.

We thank Yoo Kyung Lee for a critical reading of our manuscript. We acknowledge support from the NSF through the Center for Ultracold Atoms and Grant No. 1506369, ARO-MURI Non-equilibrium Many-Body Dynamics (Grant No. W911NF14-1-0003), AFOSR-MURI Quantum Phases of Matter (Grant No. FA9550-14-1-0035), ONR (Grant No. N00014-17-1-2253), and a Vannevar-Bush Faculty Fellowship. W.C.C. acknowledges additional support from the Samsung Scholarship.

* Present address: ColdQuanta Inc., Boulder, CO, United States of America
† Present address: Department of Physics and State Key Laboratory of Low Dimensional Quantum Physics, Tsinghua University, and Frontier Science Center for Quantum Information, Beijing, 100084, China
‡ Present address: Honeywell Quantum Solutions, Broomfield, CO, United States of America

[1] I. M. Georgescu, S. Ashhab, and F. Nori, Rev. Mod. Phys. **86**, 153 (2014).
[2] D. Jaksch and P. Zoller, Annals of Physics **315**, 52 (2005), special Issue.
[3] C. Weitenberg, M. Endres, J. F. Sherson, M. Cheneau, P. Schauß, T. Fukuhara, I. Bloch, and S. Kuhr, Nature **471**, 319 (2011).
[4] J. Schachenmayer, D. M. Weld, H. Miyake, G. A. Siviloglou, W. Ketterle, and A. J. Daley, Phys. Rev. A **92**, 041602 (2015).
[5] M. Lubasch, V. Murg, U. Schneider, J. I. Cirac, and M.-C. Bañuls, Phys. Rev. Lett. **107**, 165301 (2011).
[6] I. Bloch, J. Dalibard, and W. Zwerger, Rev. Mod. Phys. **80**, 885 (2008).
[7] J. J. García-Ripoll, M. A. Martin-Delgado, and J. I. Cirac, Phys. Rev. Lett. **93**, 250405 (2004).
[8] J. Struck, C. Ölschläger, R. Le Targat, P. Soltan-Panahi, A. Eckardt, M. Lewenstein, P. Windpassinger, and K. Sengstock, Science **333**, 996 (2011).
[9] A. de Paz, A. Sharma, A. Chotia, E. Maréchal, J. H. Huckans, P. Pedri, L. Santos, O. Gorceix, L. Vernac, and B. Laburthe-Tolra, Phys. Rev. Lett. **111**, 185305 (2013).
[10] J. Simon, W. S. Bakr, R. Ma, M. E. Tai, P. M. Preiss, and M. Greiner, Nature **472**, 307 (2011).
[11] P. Schauß, J. Zeiher, T. Fukuhara, S. Hild, M. Cheneau, T. Macrì, T. Pohl, I. Bloch, and C. Gross, Science **347**, 1455 (2015).
[12] J. Koepsell, J. Vijayan, P. Sompet, F. Grusdt, T. A. Hilker, E. Demler, G. Salomon, I. Bloch, and C. Gross, Nature **572**, 358 (2019).
[13] A. Mazurenko, C. S. Chiu, G. Li, M. F. Parsons, M. Kanász-Nagy, R. Schmidt, F. Grusdt, E. Demler, D. Greif, and M. Greiner, Nature **545**, 462 (2017).
[14] H. Sun, B. Yang, H.-Y. Wang, Z.-Y. Zhou, G.-X. Su, H.-N. Dai, Z.-S. Yuan, and J.-W. Pan, Nature Physics **17**, 990 (2021).
[15] D. Greif, G. Jotzu, M. Messer, R. Desbuquois, and T. Esslinger, Phys. Rev. Lett. **115**, 260401 (2015).
[16] J. K. Freericks and H. Monien, Europhysics Letters (EPL) **26**, 545 (1994).
[17] T. Fukuhara, P. Schauß, M. Endres, S. Hild, M. Cheneau, I. Bloch, and C. Gross, Nature **502**, 76 (2013).
[18] S. Hild, T. Fukuhara, P. Schauß, J. Zeiher, M. Knap, E. Demler, I. Bloch, and C. Gross, Phys. Rev. Lett. **113**, 147205 (2014).
[19] P. N. Jepsen, J. Amato-Grill, I. Dimitrova, W. W. Ho, E. Demler, and W. Ketterle, Nature **588**, 403 (2020).
[20] P. N. Jepsen, W. W. Ho, Amato-Grill, I. Dimitrova, E. Demler, and W. Ketterle, arXiv:2103.07866 (2021).
[21] W. C. Chung, J. de Hond, J. Xiang, E. Cruz-Colón, and W. Ketterle, Phys. Rev. Lett. **126**, 163203 (2021).
[22] H. Bernien, S. Schwartz, A. Keesling, H. Levine, A. Omran, H. Pichler, S. Choi, A. S. Zibrov, M. Endres, M. Greiner, *et al.*, Nature **551**, 579 (2017).
[23] S. Trotzky, P. Cheinet, S. Fölling, M. Feld, U. Schnorrberger, A. M. Rey, A. Polkovnikov, E. A. Demler, M. D. Lukin, and I. Bloch, Science **319**, 295 (2008).
[24] E. Altman, W. Hofstetter, E. Demler, and M. D. Lukin, New Journal of Physics **5**, 113 (2003).
[25] A. B. Kuklov and B. V. Svistunov, Phys. Rev. Lett. **90**, 100401 (2003).
[26] L.-M. Duan, E. Demler, and M. D. Lukin, Phys. Rev. Lett. **91**, 090402 (2003).
[27] D. M. Stamper-Kurn and M. Ueda, Reviews of Modern Physics **85**, 1191 (2013).
[28] A. Widera, F. Gerbier, S. Fölling, T. Gericke, O. Mandel, and I. Bloch, New Journal of Physics **8**, 152 (2006).
[29] See the Supplemental Material at [URL to be inserted] for details on the experimental setup, our fitting procedure, and the mean-field model.
[30] A. M. Kaufman, R. P. Anderson, T. M. Hanna, E. Tiesinga, P. S. Julienne, and D. S. Hall, Phys. Rev. A **80**, 050701(R) (2009).
[31] M. Greiner, O. Mandel, T. Esslinger, T. W. Hänsch, and I. Bloch, Nature **415**, 39 (2002).
[32] F. Gerbier, Phys. Rev. Lett. **99**, 120405 (2007).
[33] J. F. Sherson, C. Weitenberg, M. Endres, M. Cheneau, I. Bloch, and S. Kuhr, Nature **467**, 68 (2010).
[34] W. S. Bakr, A. Peng, M. E. Tai, R. Ma, J. Simon, J. I. Gillen, S. Foelling, L. Pollet, and M. Greiner, Science **329**, 547 (2010).
[35] A. Kleine, C. Kollath, I. P. McCulloch, T. Giamarchi, and U. Schollwöck, Phys. Rev. A **77**, 013607 (2008).
[36] C. Zener and R. H. Fowler, Proceedings of the Royal Society of London. Series A **137**, 696 (1932).
[37] L. Landau, Physikalische Zeitschrift der Sowjetunion **2**, 46 (1932).
[38] J. R. Rubbmark, M. M. Kash, M. G. Littman, and D. Kleppner, Phys. Rev. A **23**, 3107 (1981).
[39] W. S. Bakr, J. I. Gillen, A. Peng, S. Fölling, and M. Greiner, Nature **462**, 74 (2009).
[40] C. Menotti and S. Stringari, Phys. Rev. A **81**, 045604 (2010).
[41] A. J. Daley, J. M. Taylor, S. Diehl, M. Baranov, and P. Zoller, Phys. Rev. Lett. **102**, 040402 (2009).
[42] I. Morera, G. E. Astrakharchik, A. Polls, and B. Juliá-Díaz, Phys. Rev. Lett. **126**, 023001 (2021).
[43] T. Volz, N. Syassen, D. Bauer, E. Hansis, S. Dürr, and G. Rempe, Nature Physics **2**, 692 (2006).
[44] R. Grimm, M. Weidemüller, and Y. B. Ovchinnikov, Advances In Atomic, Molecular, and Optical Physics **42**, 95 (2000).

[45] F. Le Kien, P. Schneeweiss, and A. Rauschenbeutel, The European Physical Journal D **67**, 92 (2013).
[46] P. L. Gould, G. A. Ruff, and D. E. Pritchard, Phys. Rev. Lett. **56**, 827 (1986).
[47] C. Sias, H. Lignier, Y. P. Singh, A. Zenesini, D. Ciampini, O. Morsch, and E. Arimondo, Phys. Rev. Lett. **100**, 040404 (2008).
[48] R. Ma, M. E. Tai, P. M. Preiss, W. S. Bakr, J. Simon, and M. Greiner, Phys. Rev. Lett. **107**, 095301 (2011).
[49] M. P. A. Fisher, P. B. Weichman, G. Grinstein, and D. S. Fisher, Phys. Rev. B **40**, 546 (1989).